THE JOURNAL OF PHYSICAL CHEMISTRY B

Article

pubs.acs.org/JPCB

Solid-State NMR Studies of Form I of Atorvastatin Calcium

Wei David Wang,[†] Xudong Gao,[†] Mark Strohmeier,[‡] Wei Wang,*[,†] Shi Bai,*[,†,§] and Cecil Dybowski[§]

[†]State Key Laboratory of Applied Organic Chemistry, College of Chemistry and Chemical Engineering, Lanzhou University, Lanzhou, Gansu, 730000, China

[‡]Product Development, GlaxoSmithKline, Inc., 709 Swedeland Road, King of Prussia, Pennsylvania 19406, United States

[§]Department of Chemistry and Biochemistry, University of Delaware, Newark, Delaware 19716, United States

Supporting Information

ABSTRACT: Solid-state ^{13}C, ^{19}F, and ^{15}N magic angle spinning NMR studies of Form I of atorvastatin calcium are reported, including chemical shift tensors of all resolvable carbon sites and fluorine sites. The complete ^{13}C and ^{19}F chemical shift assignments are given based on an extensive analysis of $^{13}C-^{1}H$ HETCOR and $^{13}C-^{19}F$ HETCOR results. The solid-state NMR data indicate that the asymmetric unit of this material contains two atorvastatin molecules. A possible structure of Form I of atorvastatin calcium (ATC-I), derived from solid-state NMR data and density functional theory calculations of various structures, is proposed for this important active pharmaceutical ingredient (API).

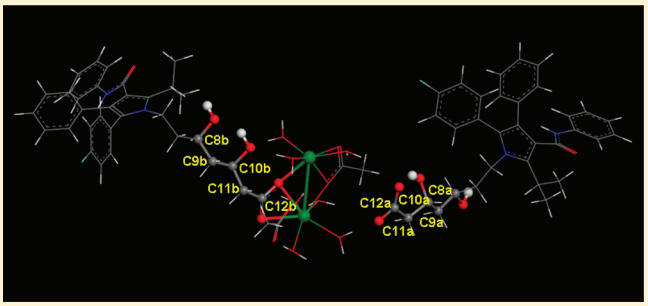

INTRODUCTION

The quality, stability, safety, and efficacy of a pharmaceutical product are dependent on its local and long-range structure in the solid state.[1] Various polymorphic forms of pharmaceutical materials typically have significantly different apparent solubilities, dissolution rates, and bioavailability.[2] These differences in physical properties have profound effects on the performance of a pharmaceutical product and the choice of the type of formulation in which a drug is administrated. Interconversion among polymorphic forms during processing, storage, and use can have detrimental effects on the drug's performance.[3] Hence, the processing, storage, and shelf life of a drug may be limited by the stability of the desired polymorphic form, and the control of the drug's form during the lifecycle of a product is critical.

Understanding the solid-state structure of these materials at the local and long-range levels is key to develop strategies for the proper administration of these drugs. Commonly used methods in the studies of polymorphic structure include X-ray powder diffraction (XRPD),[4] infrared spectroscopy (IR),[5] Raman spectroscopy (RS),[6] and solid-state nuclear magnetic resonance spectroscopy (SSNMR),[7] as well as thermal methods such as differential scanning calorimetry (DSC) and thermal gravimetry (TG).[8] The integration of all these methods provides insight into the local and long-range structure of polymorphic materials.

Atorvastatin calcium (ATC, see Figure 1), a member of a class of drugs known as statins, is commonly prescribed for lowering blood cholesterol. It acts by inhibiting 3-hydroxy-3-methyl-glutaryl-coenzyme A (HMG-CoA) reductase, an enzyme found in liver tissue that plays a central role in the production of cholesterol in the body. The structures of the catalytic portion of complexes of HMG-CoA reductase with six statins, including atorvastatin, have been analyzed in terms of this inhibition mechanism.[9] ATC is the active ingredient in Lipitor, which has become one of the best-selling drugs worldwide.

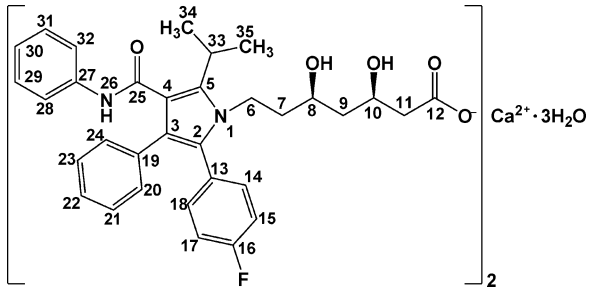

Figure 1. Molecular structure of atorvastatin, showing the numbering of the carbons and nitrogens.

Atorvastatin calcium exists in a variety of polymorphic forms. It has been reported that there are 41 crystalline forms and two amorphous forms, among which Form I of ATC (ATC-I) is the most stable crystalline form.[10] XRPD, IR, RS, DSC, and optical microscopy have been used to analyze atorvastatin calcium in tablets,[11] in crystalline and amorphous phases,[12] and in crystalline solvates.[13] Preparation and characterization of various polymorphs of atorvastatin calcium have been described

Received: December 14, 2011
Revised: February 23, 2012
Published: February 23, 2012

   dx.doi.org/10.1021/jp212074a | J. Phys. Chem. B 2012, 116, 3641−3649

in a number of patents.[14] Most of these reports have relied on characterization of ATC with XRPD, which provides predominately long-range structural information. There has been a report of the structure of a complex of atorvastatin with HMG-CoA.[9] To our knowledge, no single-crystal X-ray diffraction-based structure of Form I of atorvastatin has been reported because the polymorphs of ATC do not generally form stable crystals. Thus, extracting short-range structures of the various forms of atorvastatin presents a challenging problem that may be addressed with solid-state NMR analysis. Very few SSNMR investigations of ATC have been reported, among which are ^{13}C solid-state NMR characterizations of Form I, II, and IV reported in a patent by Briggs.[14g] Recently, solid-state ^{19}F magic angle spinning (MAS) NMR has been used to characterize amorphous forms of atorvastatin in dosage formulations.[15]

Solid-state NMR parameters are uniquely sensitive to the local structure in polymorphic systems such as pharmaceutical solids.[7,16] Most studies of pharmaceutical solids have been based on known single crystal X-ray structures, with a few exceptions,[16a,17] where X-ray powder diffraction or neutron diffraction techniques were used to provide initial structural parameters for prediction of NMR parameters. It is, therefore, challenging to investigate structure characteristics without prior knowledge of the X-ray structure, particularly for polymorphic materials with large numbers of carbons and heteroatoms.

In this report, we analyze the local structure of the most stable Form I of atorvastatin calcium (ATC-I) using solid-state NMR spectroscopy without available single-crystal X-ray data as a structural reference. The isotropic NMR chemical shift, obtained by the MAS technique, is extremely sensitive to polymorphic structure in solids. It provides a global representation of the local electronic structure. In addition, the principal values of the chemical shift tensor at each carbon site provide information on the geometry of the electronic distribution about the nuclear centers, something that cannot often be directly determined from a simple MAS experiment for a complex molecule like ATC. Nuclear dipole−dipole couplings among nuclei give direct information on internuclear distances, which can be used to infer local structure.[18] Experimentally determined dipolar interactions, in turn, provide critical hints in spectral assignments.[16i]

Form I of ATC has a complex solid-state ^{13}C NMR spectrum, with a total of 33 carbons and asymmetric doubling for several positions. We provide the first complete ^{13}C, ^{19}F, and ^{15}N isotropic chemical shift assignments for ATC-I that demonstrate the existence of two molecules in the asymmetric unit. We suggest the use of the chemical shift difference between carbons of the two molecules in the asymmetric unit as a benchmark to evaluate proposed local structure used in DFT calculations of the NMR parameters. For certain carbon sites, where the CP/MAS resolution permits extraction of the full tensor, the ^{13}C chemical shift tensors have also been measured. The integration of these experimental NMR data with density functional calculations on model local structures, along with XRPD, SEM, and thermal analyses, allows us to propose a possible local structure of this important active pharmaceutical ingredient.

EXPERIMENTAL SECTION

Sample Preparation. Atorvastatin calcium $(C_{33}H_{34}O_5N_2F)_2Ca{\cdot}3H_2O$ was purchased from Quzhou Aifeimu Chemical Co., Ltd., Zhejiang, China. The purity is greater than 99.1%. The sample was verified by solution ^1H and ^{13}C NMR and was used for all measurements without further purification.

Deuterated ATC-I was prepared first by mixing atorvastatin acid (196.2 mg) with D_2O (20 mL). This solution was slowly added to a CaO suspension of 9.86 mg in 1.5 mL of D_2O. The mixture was then heated to 70 °C and continuously stirred for 1.5 h at this temperature. After slowly cooling down to room temperature, the mixture was filtered and washed with diethyl ether three times. The sample was dried at room temperature for 2 days (131 mg, 61% yield).

Scanning Electron Microscopy (SEM). The morphology and particle size distribution of the sample were studied using scanning electron microscopy (HITACHI S-4800 Electron Microscopy). The sample was dispersed in *n*-hexane and mounted on silicon stubs. After evaporation of the *n*-hexane, the sample was sputter-coated with a thin layer of gold at 10 Pa using the HITACHI E-1045 ion sputterer. The specimens were scanned with a 25 kV electron beam.

X-ray Powder Diffraction (XRPD). X-ray powder diffraction (XRPD) patterns of the sample were recorded at room temperature (298 K) on a PANalytical X'Pert PRO diffractometer with Cu Kα radiation (1.54 Å), at 40 kV and 40 mA. The XRPD scans were recorded in continuous mode with a step size of 0.02° and step time of 10 s, over a 2θ range of 3−45°.

Differential Scanning Calorimetry (DSC) and Thermogravimetric Analysis (TGA). DSC and TGA were performed simultaneously using a Linseis STA PT 1600 system. ATC sample (11.40 mg) was weighed and analyzed with a heating rate of 20 °C/min from 30 to 800 °C and a purging of nitrogen gas (20 mL/min).

NMR Spectroscopy. ^{13}C and ^{15}N CP/MAS experiments were carried out with a Bruker AVANCE II WB400 NMR spectrometer, operating at a proton frequency of 400.13 MHz. Samples were packed in 4 mm rotors, a double-resonance (HX) probe was used, and all spectra were obtained at 298 ± 2 K. The CP/MAS experiments were carried out with a sample spinning rate of 10 000 ± 2 Hz, unless otherwise noted. TPPM[19] decoupling during CP/MAS data acquisition was provided by a 104.2 kHz proton decoupling field. For most ^{13}C and ^{15}N CP/MAS spectra, the contact time was 3 ms. For ^{13}C CP/MAS experiments carried out with nonquaternary-carbon suppression (NQS),[20] a 40 μs delay was used to suppress the contributions of carbons adjacent to protons. All ^{13}C chemical shifts were referenced externally via the resonance of adamantane at an isotropic chemical shift relative to tetramethylsilane (TMS) of 38.55 ppm. The ^{15}N chemical shifts were referenced externally via the resonance of glycine (^{15}N-labeled) at an isotropic chemical shift of 10.0 ppm.

Two-dimensional $^{13}C-^1H$ HETCOR experiments[21] were performed with a spinning rate of 10 000 ± 2 Hz on the same instrument. The TPPM decoupling field strength was 104.2 kHz, with a pulse delay of 3.0 s. A Lee−Goldburg $^1H-^1H$ decoupling scheme[22] was used during the evolution period, which consisted of a 2.3 μs $\pi/2$ ^1H pulse and four Lee−Goldburg cycles per evolution increment. Eighty evolution points, each with 320 scans, were collected. The ^1H dimension was referenced internally to the methyl group of Form I at 0.5 ppm, as determined with ^1H MAS NMR spectroscopy. The ^{13}C dimension was referenced externally to the resonance of adamantane at 38.55 ppm. All reported proton shifts were scaled by 0.578, the expected scaling for Lee−Goldburg

dx.doi.org/10.1021/jp212074a | J. Phys. Chem. B 2012, 116, 3641−3649

homonuclear decoupling. The data were processed by multiplication by a cosine-square function in the t_1 and t_2 dimensions prior to Fourier transformation.

To determine chemical shift tensors (CSTs), we used the 2D-SUPER experiment.[23] In a typical 2D-SUPER experiment, the sample was spun at a frequency of 5000 ± 2 Hz and 2000 ± 2 Hz for the aromatic range and aliphatic range, respectively, which dictates the 2π pulse lengths for chemical-shift recoupling. The proton decoupling amplitude during the recoupling section of the experiment was 116.8 kHz. For each t_1 increment, 2048 complex points were collected along the acquisition (isotropic) dimension. Depending on the signal-to-noise ratio, either 512 or 1024 scans were coadded. Sixty-four complex points along the F_1 (anisotropic) dimension were used. The recoupling section was followed by a γ-integral delay of 1 ms to eliminate spinning sidebands in the F_1 dimension. A TOSS sequence[24] was used to suppress spinning sidebands in the F_2 dimension. The scaling factor for the SUPER experiment was 0.155. A cosine-square function was applied to both the t_1 and t_2 dimensions prior to Fourier transformation. Subsequently, spectra were repeatedly sheared along the F_1 dimension until the anisotropic chemical-shift patterns were centered in the spectrum along the F_1 dimension. To determine the chemical shift tensor fully, the appropriate spectral slice was fitted with the line-shape-analysis package of Bruker's TopSpin software. The referencing of the extracted chemical-shift pattern was based on its corresponding isotropic shift in the F_2 dimension.

The ^{19}F CP/MAS spectrum was obtained on a Bruker Avance II NMR spectrometer operating at a proton frequency of 500.13 MHz. The sample temperature was controlled at 273 ± 1 K, while the sample spinning rate was regulated at 12 500 ± 2 Hz. The ^{1}H TPPM decoupling scheme was used during CP/MAS data acquisition with a decoupling power of 102.0 kHz. A ^{1}H−^{19}F contact time of 2 ms and a recycle delay of 3 s were used. All ^{19}F chemical shifts were referenced externally via the resonance of flurbiprofen [(*RS*)-2-(2-fluorobiphenyl-4-yl)propanoic acid] at an isotropic chemical shift of −115.0 ppm.[25]

Two-dimensional ^{13}C−^{19}F HETCOR experiments[26] were performed at a spinning rate of 8000 ± 2 Hz on a Bruker 500 MHz NMR spectrometer. The ^{1}H−^{19}F and ^{19}F−^{13}C contact times were set to 4 ms. A TPPM scheme was used as the proton decoupling with a decoupling power of 102.0 kHz in both the ^{19}F evolution and ^{13}C acquisition dimensions. The ^{19}F−^{13}C dipolar coupling was suppressed during the ^{19}F evolution and ^{13}C acquisition dimension using π-decoupling. All ^{19}F data were acquired with a 4.0 mm triple-resonance (HFX) probe.

Solution NMR spectra were obtained on a Bruker AVANCE III 400 MHz NMR spectrometer.

DFT Calculations. The DFT calculations were performed with the Gaussian09 software package[27] at the B3LYP level of theory with a basis set of 6-31G(d). For the geometry optimization, the 3-21G basis set was chosen. The calculated ^{13}C chemical-shift parameters were referenced to the isotropic position of tetramethylsilane (TMS), obtained at the same level of theory and with the same basis sets.

RESULTS AND DISCUSSION

Characterization of ATC-I. The microphotograph (see Figure S1 in Supporting Information) of the sample as received showed primarily rod-shaped crystals, similar to what has been previously observed for ATC-I.[12] The XRPD pattern (see Figure S2 in Supporting Information) showed characteristic peaks at 2θ of 9.01°, 9.32°, 10.14°, 10.44°, 11.72°, 12.06°, and 16.89°, in agreement with previously reported patterns[12,14g] for ATC- I. The lack of other peaks in the XRPD spectrum further verified the purity of the sample. The TGA analysis indicated a water content of 4.56% w/w, which matched well with a theoretical water loss for trihydrated ATC of 4.47% w/w.[28] The DSC analysis (Figure S3, Supporting Information) showed a broad endotherm from water loss in the temperature range of 80−125 °C and a second endotherm for water loss and melting in the temperature range of 140−180 °C. The SEM, XRPD, TGA, and DSC data all indicated that the polymorph of ATC in this sample as received is Form I of atorvastatin calcium.

Chemical Shift Assignments of ATC-I. An accurate and complete assignment of chemical shifts of ATC-I is essential to the analysis of SSNMR data in terms of the local three-dimensional structures of polymorphs. The ^{13}C CP/MAS spectrum of ATC-I is given in Figure 2. It can be seen from

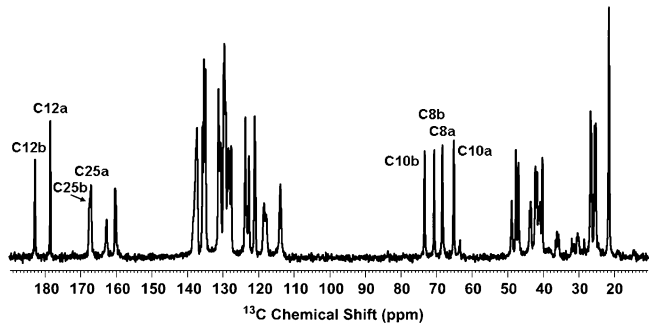

Figure 2. CP/MAS spectrum of ATC-I. Some doubled carbon peaks are labeled. All other assignments can be found in Table 1.

Figure 2 (and Table 1) that a number of carbon sites in ATC-I have two distinguishable peaks in the solid-state NMR spectrum. A solution ^{13}C spectrum (see Figure S4 in Supporting Information) shows only single resonances because isotropic molecular tumbling motion in solution makes the two sites, on average, equivalent. The doubled resonances in the solid-state spectrum imply that two molecules coexist in the asymmetric unit,[7a,16d] where chemical shift differences are ascribable to the asymmetric crystal packing in the solid. Typically, ^{13}C chemical shift differences due to crystal packing are in the range of 0.1 to a few parts per million.[7a] In the case of ATC- I, differences (ranging from a few parts per million to as high as 8.2 ppm) are consistently large, indicating the presence of strong intermolecular and intramolecular interactions. These interactions may be electrostatic interactions between the calcium ion and the carboxyl groups of ATC, or they may be intermolecular or intramolecular hydrogen bonding.

We measured ^{1}H−^{13}C HETCOR spectra at two different contact times (50 and 300 μs) to assign all chemical shifts of the complex ^{13}C spectrum of ATC-I reliably. The short-contact-time sequence provided correlations between directly bonded nuclei, and the long-contact-time sequence provided possible long-range correlations such as the dipolar coupling of the hydroxyl proton to the carbon to which the hydroxyl group is bonded. The incomplete published assignments[14g] of the ^{13}C chemical shifts for ATC-I (c.f. Table 1) are inconsistent with the ^{13}C−^{1}H HETCOR data. As an example, consider the

dx.doi.org/10.1021/jp212074a | J. Phys. Chem. B 2012, 116, 3641−3649

Table 1. Solid-State NMR Chemical Shift of ATC-I[a]

assignment this work	a				previous assignment[c]	b				previous assignment[c]
	δ_{11}	δ_{22}	δ_{33}	δ_{iso}[b]		δ_{11}	δ_{22}	δ_{33}	δ_{iso}	
C2				128.51					128.17	
C3				123.63					123.63	
C4				122.57					120.92	
C5				137.19					137.82	
C6	67.4	43.9	18.6	43.30	n/a	62.6	38.4	20.8	40.68	n/a
C7	61.5	45.6	13.0	40.02	C6, C7, C9, or C11	63.9	43.7	18.4	41.97	C6, C7, C9 or C11
C8	95.9	73.4	35.0	68.12	C8 or C10	99.8	71.7	40.6	70.45	C8 or C10
C9	57.2	54.8	28.2	46.73	n/a	52.7	47.0	24.9	41.53	n/a
C10	93.0	66.7	35.1	64.90	C8 or C10	94.0	81.9	43.4	73.11	C8 or C10
C11	65.7	58.5	17.9	47.41	C6, C7, C9, or C11	62.1	55.4	28.3	48.60	n/a
C12	231	195.1	109.5	178.46	C12 or C25	238.5	207.3	102.6	182.74	C12 or C25
C13				129.69					129.10	
C14				130.50					130.74	
C15				113.90					113.68	
C16				160.19/162.70	n/a				160.04/162.58	n/a
C17				113.90					113.68	
C18				130.50					130.74	
C19				135.58					135.23	
C20				131.09					131.09	
C21				129.47					129.47	
C22				123.63					123.63	
C23				129.47					129.47	
C24				131.09					131.09	
C25	246.0	159.4	95.6	167.07	C16	247.1	159.1	95.1	167.49	C16
C27				135.23					134.79	
C28				118.28					117.76	
C29				127.56					127.56	
C30				123.22					123.22	
C31				127.56					127.56	
C32				118.28					117.76	
C33	37.3	24.6	17.1	26.25	C33	37.3	24.6	17.1	26.41	C33
C34	37.9	13.7	12.1	21.23	C33	37.9	13.7	12.1	21.27	C33
C35	42.8	32.8	−0.3	24.97	C35	42.8	32.8	−0.3	25.26	C35
F	−59.6	−130.2	−162.5	−117.41		−64.2	−127.5	−165.9	−119.19	
N1				132.0					130.8	
N26				119.2					119.2	

[a] ^{13}C chemical shift tensor elements were measured using a 2D-SUPER method, and ^{19}F chemical shift tensor components were obtained by fitting the spinning sideband of the CP/MAS spectrum. The uncertainty in chemical shift tensor components is estimated to be ±3 ppm. [b] Isotropic values from CP/MAS experiments with an uncertainty of ±0.05 ppm. [c] The previous assignments are from a patent;[14g] resonances in the range of 113.8 to 137.0 ppm were assigned as aromatic carbons.

assignments of C12, C16, and C25 (eight resolved peaks between 155 and 185 ppm). Previously, the ^{13}C peaks at 182.74 and 178.46 ppm were assigned to be C12 or C25. We assign these two peaks to the resonances of C12 of two atorvastatin molecules in an asymmetric unit (C12b and C12a) because the HETCOR cross-peaks are observed to correlate these carbon peaks to the proton signal of C11 approximately at 2.5 ppm (Figure 3). The ^{13}C resonances at 174.46 ppm and at 182.74 ppm were labeled as C12a and C12b, respectively, to differentiate two C12 sites in the asymmetric unit. Two peaks at 167.49 and 167.07 ppm were previously assigned to be from C16. However, Figure 3 shows clearly that these two resonances have cross-peaks with the proton signal around 9 ppm, which is an amide proton (NH) signal. For this reason, these peaks can unambiguously be assigned to C25b and C25a, respectively. The separation between these two peaks was wrongly considered as the $^{13}C-^{19}F$ scalar coupling between C16 and the fluorine nucleus.[14g] Our solution ^{19}F and ^{13}C NMR data (data not shown here) indicate that the $^{13}C-^{19}F$ scalar coupling is 245 Hz. In fact, the peaks at 162.70/162.58 and 160.19/160.04 ppm were found to be approximately 250 Hz from each other, in good agreement with the $^{19}F-^{13}C$ scalar coupling constant found in solution NMR data. Preliminary analysis indicates that the two sets of doublets at 162.70/160.19 and 162.58/160.04 ppm belong to two distinct resonances of C16 (See Figures 3 and 5), which is further verified by the $^{13}C-^{19}F$ HETCOR data as discussed in detail later.

By the same strategy, all carbon chemical shifts of ATC-I were assigned. In addition to the $^{13}C-^{1}H$ HETCOR experiment, the chemical shift assignments in the aromatic range (110 to 140 ppm) were also aided by comparing the CP/MAS spectrum with an NQS-CP/MAS spectrum to identify quaternary carbons (data not shown here). The detailed assignments of C6 to C12, C33−C35, and aromatic carbons

dx.doi.org/10.1021/jp212074a | J. Phys. Chem. B 2012, 116, 3641−3649

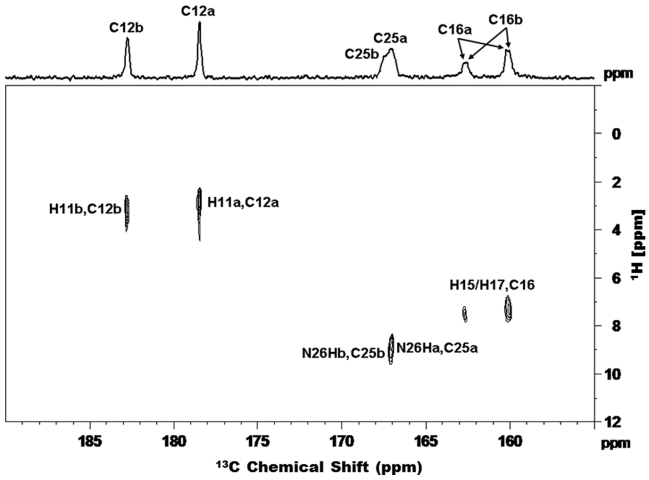

Figure 3. Section of the ^{13}C−^{1}H HETCOR spectrum of ATC-I taken with a contact time of 300 μs.

can be found in Figures S5, S6, S7 and Table S1 in the Supporting Information. The complete assignments of the isotropic chemical shifts and the resolvable chemical shift tensors of ATC-I are tabulated in Table 1.

In addition to ^{13}C CP/MAS analysis, a ^{19}F CP/MAS spectrum was obtained for ATC-I, shown in Figure 4. Two distinguishable resonances are seen, indicating two fluorine sites in ATC-I. The ^{19}F chemical shift assignments were made possible by the ^{13}C−^{19}F HETCOR experiment at a mixing time of 4 ms. The ^{13}C−^{19}F HETCOR cross-peaks in Figure 5 show correlations between Fa at −117.36 ppm and C16a at 161.45 ppm (an average of 162.70 and 160.19 ppm). Similarly, Fb at −119.16 ppm is coupled to C16b at 161.31 ppm (an average of 162.58 and 160.04 ppm). The correlations between Fb and C15/17b, and between Fa and C15/17a, were observed, along with weak correlations between Fa and C13a, C14a, and C18a.

Chemical shift tensors for the two fluorine sites were determined through Herzfeld−Berger analysis[29] of the spinning sideband patterns of the two resonances, as indicated by the blue dotted line in Figure 4. The resulting chemical shift tensors are listed in Table 1.

^{15}N CP/MAS spectra of deuterated and undueterated ATC-I are shown in Figure 6. The two peaks at 130.8 and 132.0 ppm were assigned to the pyrrole nitrogen (N1) of the two atorvastatin molecules. The resonance at 119.2 ppm, with an integral of nearly twice that of N1, is assigned to the amide nitrogen (N26), which must have identical chemical shift parameters on the two distinct atorvastatin molecules. The ^{15}N assignment of this latter resonance to the amide site is based on the fact that in deuterated ATC-I it vanishes because of deuterium exchange. It is conceivable that the ^{15}N chemical shift difference of N26 in the two atorvastatins is averaged out due to a rapid rotation of the amide bond, showing only a single resonance representing the two different sites. The doublings observed in the fluorine and nitrogen spectra, once again, indicate that there are two atorvastatins in the asymmetric unit, not one.

Structure of ATC-I. Since the crystal structure of ATC-I is not available, the three-dimensional molecular structure of atorvastatin calcium in the solid state is unknown. In this section, we describe a possible local structure of ATC-I based on the simultaneous interpretation of the experimental solid-state NMR data and DFT calculations.

Figure 7 shows the difference in isotropic ^{13}C chemical shifts of each carbon site between the two independent molecules in the asymmetric unit, defined as $\Delta\delta = \delta_a - \delta_b$, (a and b represent a and b molecules, respectively). Atorvastatin a is the molecule that more closely resembles the solution structure than does b, based on the smaller root-mean-square deviation of its isotropic shifts from solution shifts. From Figure 7, one can discern a large oscillation of the difference between the two molecules for carbons C4 to C12, suggesting that in this region the two atorvastatin molecules have different NMR chemical shifts, possibly due to hydrogen bonding of hydroxyl groups or difference in electrostatic charge distribution in the vicinity of calcium ions in the solid structure, apart from the crystal packing effect. This variation of the difference with position serves as a benchmark in evaluating structural models based on predicted chemical shifts from the DFT calculations. The benchmark therefore consists of the results of 66 unique chemical shift measurements (2 times 33 chemical shifts) and is statistically significant. More importantly, the comparison of differences in chemical shifts allows us to eliminate possible inaccuracies that might arise from offsets in the DFT calculations or the choice of basis sets.

As discussed above, the doubling in the NMR spectra clearly indicates that the asymmetric unit contains two atorvastatin molecules. To construct an initial model for DFT calculations, we examined a large number of organic calcium salts in the Cambridge Structure Database (CSD) that satisfied the

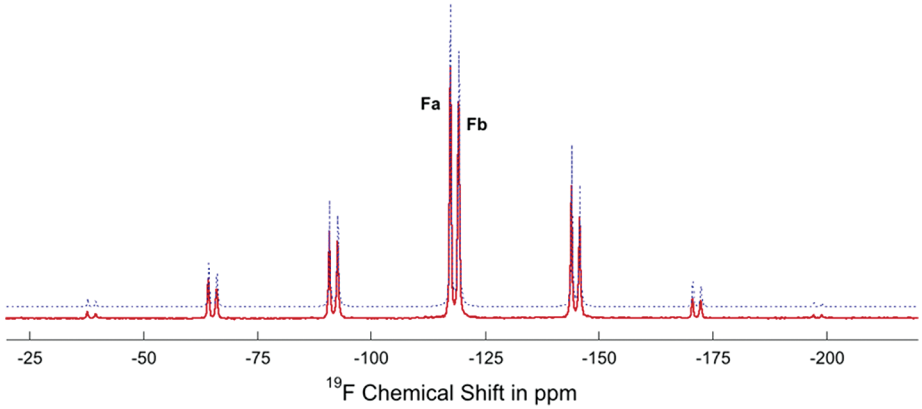

Figure 4. ^{19}F CP/MAS spectrum of ATC-I taken with a spinning rate of 12.5 kHz. The experimental spectrum (red) was obtained by applying 30 Hz line broadening. The blue dotted line represents the line shape analysis using the Herzfeld−Berger technique.

dx.doi.org/10.1021/jp212074a | J. Phys. Chem. B 2012, 116, 3641−3649

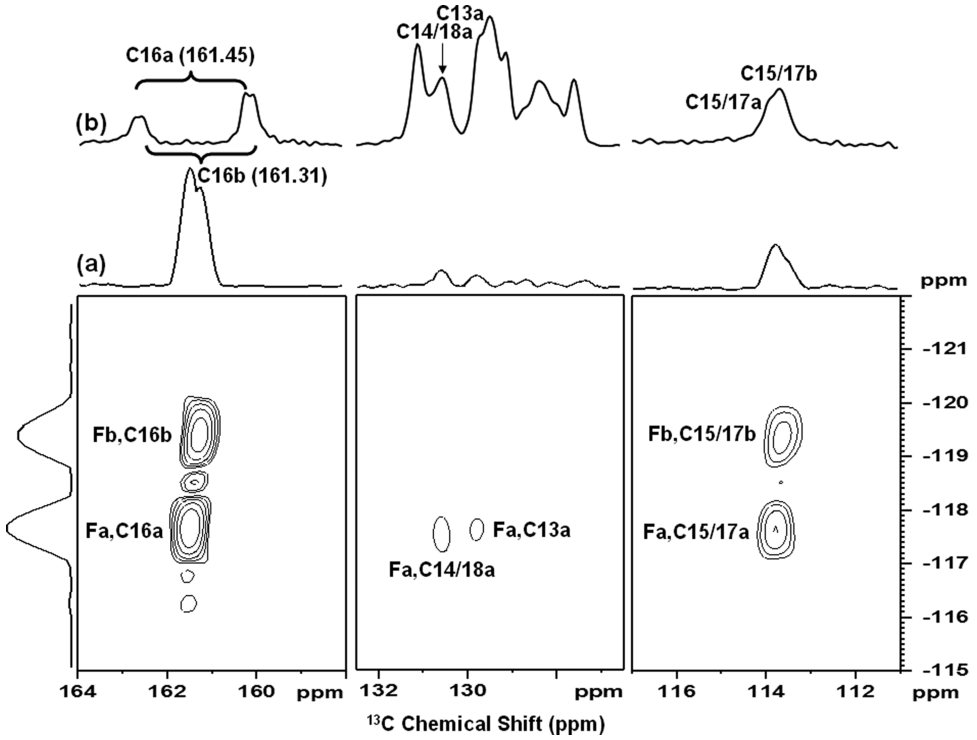

Figure 5. Sections of the $^{13}C-^{19}F$ HETCOR spectrum taken with a contact time of 4 ms. (a) The projection of 2D spectrum along the ^{19}F dimension. (b) ^{13}C CP/MAS spectrum, which shows the $^{19}F-^{13}C$ scalar coupling for site C16.

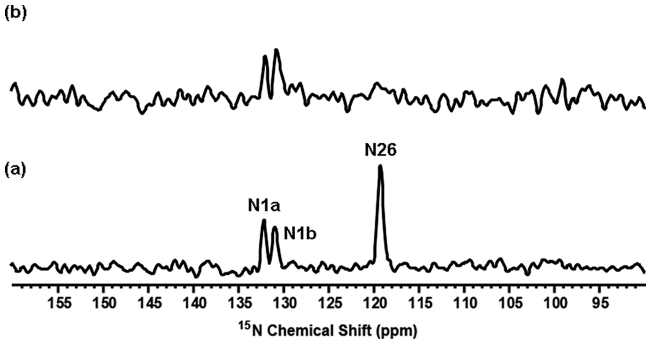

Figure 6. ^{15}N CP/MAS spectra for ATC-I (a) and deuterated ATC-I (b). The signal of N26 disappears in panel b due to deuterium exchange of the labile amide protons.

following criteria: (1) having similar calcium−oxygen coordinations and (2) having a similar hydrate in the crystal form as ATC-I. Calcium benzoate ($Ca(C_6H_5COO)_2{\cdot}3H_2O$) was chosen because it meets the criteria. In calcium benzoate (CSD code JEDCOK01[30]), four benzoic acids, along with waters of hydration, are coordinated to two calcium ions, in which two benzoic acid molecules are closer to the ions than the others. To build the initial model of ATC-I, two of the four benzoic acid molecules, one closer to and another father away from the calcium cluster, in the calcium benzoate structure were replaced by atorvastatins, whose initial structure was taken from the reported HMG-CoA reductase-atorvastatin complex,[9] while keeping all oxygens of the carboxyl group (COO−) at the same or similar positions. To simplify the model such that the calculation is feasible, the other two symmetric benzoic acid molecules in calcium benzoate were replaced with acetic acid molecules. The oxygens of the acetic acids were placed in the same or similar positions as in calcium benzoate.

From this initial model, we made modifications to the structure of the atorvastatins based on the solid-state $^{13}C-^{1}H$

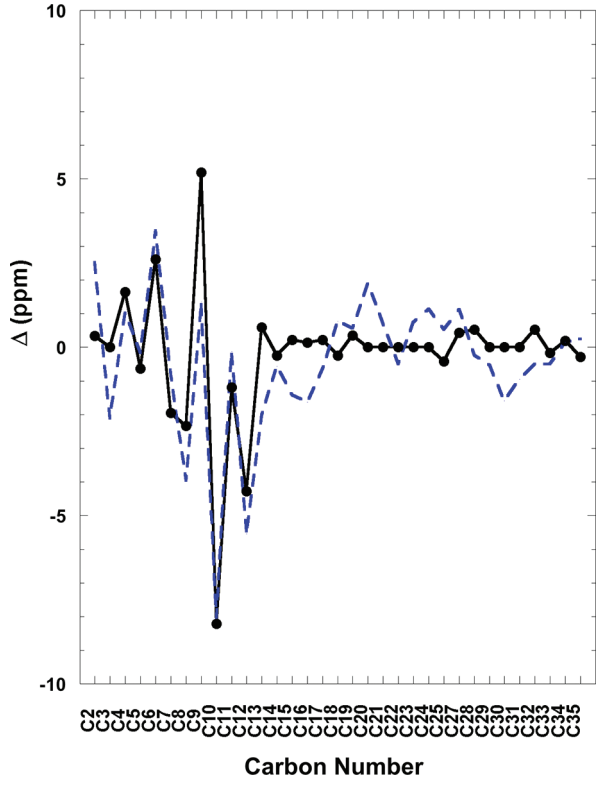

Figure 7. Chemical shift difference between atorvastatin a and b. The calculated chemical shift differences based on the proposed model (blue dashed line) are compared with experimental values (●). The carbon numbering is given in Figure 1.

dx.doi.org/10.1021/jp212074a | J. Phys. Chem. B 2012, 116, 3641−3649

HETCOR spectra. For atorvastatin a, a cross-peak between C11 and the hydroxyl proton of C10 (Figure S5 in the Supporting Information) is observed, which indicates the hydroxyl proton of C10 is pointing toward the direction of C12. In addition, a much stronger cross-peak between C7a and C8-OHa than that of C9a and C8-OHa is observed, implying that the hydroxyl proton of C8 points toward C7. However, for atorvastatin b, the cross-peaks observed for C9/C10-OH and C7/C8-OH, but not for C11/C10-OH, shown in Figure S5 (Supporting Information), indicated that the hydroxyl protons of C8 and C10 are pointing in the same direction. The modified arrangement of hydrogen groups for atorvastatins a and b is presented in Figure 8.

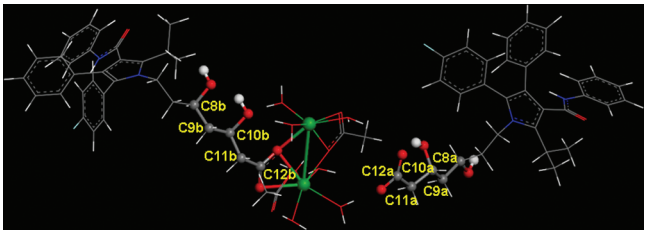

Figure 8. Proposed local structure of atorvastatin, showing that the orientations of the hydroxyl groups are different in atorvastatin a and b.

The geometry of the modified structure was optimized using the B3LYP/3-21G basis set. Subsequently, we used the more complete B3LYP/6-31G(d) basis set in the calculation of ^{13}C chemical shifts of the atorvastatins. The calculated chemical shift differences between molecules a and b are shown in Figure 7 as the blue dashed line.

The proposed model generally reflects the trend of chemical shift differences observed experimentally as a function of the carbon number. In particular, it predicts the large amplitude oscillation of the difference for carbons between C4 and C12, which probably reflects the structure due to hydrogen bonding of the hydroxyl groups of C8 and C10 as well as the electrostatic effects of the calcium ions. Although a relatively small oscillation is predicted between C13 to C35 compared with the oscillation observed in the range of C4 to C12, the theoretical curve shows larger-amplitude fluctuations than seen experimentally for carbons in this range. A large number of aromatic carbons (C13−C18, C19−C24, and C27−C32) reside in this range, and the effects of aromatic ring currents from adjacent molecules in this crystalline environment can hardly be accounted for by a calculation that is primarily for a gas-phase environment, as this one is. We believe the general outlines of the proposed structural model for the local structure of ATC-I (shown in the .mol format in the Supporting Information) are statistically reasonable and consistent with the NMR data.

To examine the sensitivity of the present method, we first used the same procedure in generating the proposed model, except we do not alter the orientation of the hydroxyl groups. This test structure (Model I) is an arrangement as if the solid-state $^{13}C-^{1}H$ HETCOR data were not utilized to modify the local structure. The geometry optimization and chemical shift calculations were performed as before. The theoretical curve (red dotted line) obtained in this manner failed to reproduce the experimental observations (Figure S8, Supporting Information), both in the aliphatic chain and in the aromatic ring ranges. In a second attempt, we started with the crystal structure of calcium acetate[31] as an initial model, replacing the acetic acid molecules with atorvastatin molecules (the structure being obtained from the enzyme complex without altering the orientation of hydroxyl groups). We called this arrangement Model II. The theoretical curve (blue dashed line in Figure S8, Supporting Information) obtained in this way completely failed to predict the experimental observations (Figure S8, Supporting Information). To compare models in a more quantitative manner, we defined a total square root square deviation of the model from experiment.

$$d = \sqrt{\sum (\Delta_{exp} - \Delta_{DFT})^2}$$

where Δ_{exp} and Δ_{DFT} are isotropic chemical shift differences obtained from experimental measurements and DFT calculations for ATC-I, respectively. This difference, in units of ppm, represents the overall quality of a model. The d values for Model I and Model II are 15.49 and 16.18 ppm, respectively. This deviation was only 7.03 ppm for the model of Figure 8. We conclude that the local structural model of Figure 8 is far superior in reproducing the NMR observations than either Model I and Model II. These simple tests show that the proposed method for exploring the local structure is very sensitive to the structure. In this case, the orientations of the hydroxyl group suggested by solid-state NMR data, which affect hydrogen bonding structure, are critical in the model for predicting chemical shifts of ATC-I.

For Form I of atorvastatin calcium, the calcium cation orients two atorvastatin molecules such that the structure is relatively rigid. For a more flexible system where more than one molecule exists in an asymmetric unit, a larger set of molecular models should be considered for the DFT calculation.

Chemical Shift Tensors of ATC-I. The isotropic NMR chemical shift is an average of three principal values of the chemical-shift tensor. The principal values, δ_{11}, δ_{22}, and δ_{33}, of the symmetric second-rank chemical-shift tensor (CST) provide more details about the electronic environment in three dimensions. There are several methods[23,32] for measuring the principal values for systems containing multiple nuclear sites using the magic angle spinning technique. In this report, we used the 2D-SUPER experiment[23] to measure the ^{13}C chemical shift tensors of all resolvable carbon resonances of ATC-I. The results are listed in Table 1. Once again, at this high level of comparison, the model of Figure 8 gives an excellent linear correlation between the measured and calculated principal values of the chemical shift tensors (see Figure S9 in the Supporting Information).

Considering the experimental errors involved in measurement of a chemical shift tensor, the differences of the principal values of C6, C7, and C8 between atorvastatins a and b are relatively insignificant, reflecting the similar electronic environment near these carbon sites, something that is generally consistent with the proposed model. However, the electronic environments near C9 and C10 are found to be quite different. A change in chemical shift of approximately 14 ppm was found for C10 between a and b, which is probably due to the fact that, in our model, the orientation of the hydroxyl group on C10 in atorvastatin a is opposite to that in b.

In principle, the direction of the principal axes of the chemical shift tensor in the molecular frame cannot be determined experimentally from measurements on powdered samples, except in certain situations required by symmetry.

dx.doi.org/10.1021/jp212074a | J. Phys. Chem. B 2012, 116, 3641−3649

However, it is well-known that the principal axes of the chemical shift tensors of carboxyl and carbonyl carbons are consistently observed to be related to the molecular frame. The 22 axis is always nearly collinear with the direction of the double bond (C═O). The 11 axis, lying approximately in the plane of the carboxyl group, is perpendicular to the 22 axis. The 33 axis is thus perpendicular to the plane defined by the 11 and 22 axes.[33] From Table 1, we note that the experimental value of δ_{22} for C12 is shifted from 207 ppm for atorvastatin b to 195 ppm for atorvastatin a. We ascribe this 12 ppm shift to the distance difference of a and b from the calcium cluster. It has been reported[33b] that stronger hydrogen bonding is associated with increased shielding in δ_{22} of deprotonated carboxylates. In the proposed model, the hydroxyl OH on C10 points to carboxyl oxygens on C12 in atorvastatin a, which leads to stronger hydrogen bonding of the carboxyl oxygen compared to that in molecule b. A 12 ppm increased shielding of δ_{22} of C12 from b to a is consistent with this local structure of the model. For C25, there are no significant changes in the chemical shift tensor between a and b, consistent with the observation that ^{15}N chemical shifts of N26 for the two atorvastatin molecules are indistinguishable. The average effect resulting from rapid amide bond rotation may also contribute to the fact that there are only small chemical shift differences in C25 in the two molecules.

The chemical shift span, $|\delta_{33}-\delta_{11}|$, is sometimes used as an index of slow molecular motion near the nuclear site. From Table 1, it can be seen that the ^{13}C and ^{19}F spans of selected sites in the two atorvastatins in ATC-I are comparable, indicating these two atorvastatin molecules have similar molecular motion characteristics in the asymmetric unit.

CONCLUSIONS

Form I of atorvastatin (ATC-I) has been studied using solid-state NMR spectroscopy, DFT calculations, X-ray powder diffraction, and thermal analysis techniques. We have given a complete assignment of ^{13}C, ^{15}N, and ^{19}F solid-state chemical shifts of this important active pharmaceutical ingredient through a careful and extensive analysis of the experimental CP/MAS and two-dimensional correlation data. In addition to isotropic chemical shifts, the ^{13}C chemical shift tensors of resolvable resonances (C6−C12, C25, and C33−C35) and fluorine site of ATC-I have been reported.

Without recourse to an X-ray crystal structure for this solid, we propose a local structure consistent with solid-state NMR data and DFT calculations. In this structure, two atorvastatin molecules are in the asymmetric unit, in agreement with the experimentally observed doubling of resonances for a number of carbon sites, fluorine sites, and the amide nitrogen site. The calculated chemical shift differences based on the proposed structure are in good agreement for a total of 66 chemical shift measurements. Specifically, the suggested orientations of hydroxyl groups, and therefore the hydrogen bonding structures, are reflected in the calculated chemical shift parameters.

The proposed model and its agreement with the solid-state NMR spectroscopy of ATC-I give insight into how one might determine local structure without knowledge of X-ray structure. Other seemingly reasonable models that we tried do not reproduce the NMR data as well as the proposed model. This comparison shows that NMR parameters sensitive to local conformation and structure may provide information on structure, even when a definitive X-ray structure is not available.

A recent study[34] using ^{43}Ca solid-state NMR of an enriched calcium biological model compound revealed details on the electronic environment of the calcium site through the effects of structure on the magnitude and orientation of the ^{43}Ca chemical shift and quadrupolar tensors. Given that ATC-I contains calcium sites, one would expect that an extended investigation using ^{43}Ca solid-state NMR spectroscopy would provide even more detailed structural information on ATC-I.

ASSOCIATED CONTENT

Supporting Information

SEM microphotograph of ATC-I. XRPD, TGA, DSC, solution ^{13}C NMR spectrum, and ^{13}C−^{1}H and ^{13}C−^{19}F HETCOR spectra. Chemical shift difference vs carbon number for models I and II. Experimental chemical shift tensor components vs calculated chemical shift tensor components. Proposed model in .mol format. This material is available free of charge via the Internet at http://pubs.acs.org.

AUTHOR INFORMATION

Corresponding Author

*E-mail: bais@udel.edu (S.B.); wang_wei@lzu.edu.cn (W.W.).

Notes

The authors declare no competing financial interest.

ACKNOWLEDGMENTS

We thank Professor Tu Yong-Qiang of Lanzhou University for suggesting atorvastatin calcium as an important pharmaceutical solid for study. Mr. Zhu Junling is acknowledged for his help on the DFT calculations. We thank Dr. Liu Wei for insightful discussion concerning the research reported here. This work was supported by the National Natural Science Foundation of China (21075057 and 20933009). C.D. acknowledges the support of the National Science Foundation under Grant CHE-0956006.

REFERENCES

(1) Guidance for Industry ANDAs: Pharmaceutical Solid Polymorphism; U.S. Department of Health and Human Services, Food and Drug Administration, Center for Drug Evaluation and Research: Rockville, MD, July 2007.

(2) Brittain, H. G.; Grant, D. J. W. *Effect of Polymorphism and Solid-State Solvation on Solubility and Dissolution Rate*; Marcel Dekker, Inc: New York, 1999.

(3) Byrn, S. R.; Pfeiffer, R. R.; Stowell, J. G., *Solid-State Chemistry of Drugs*, 2nd ed.; SSCI, Inc.: West Lafayette, IN, 1999.

(4) Dong, W.; Gilmore, C.; Barr, G.; Dallman, C.; Feeder, N.; Terry, S. *J. Pharm. Sci.* **2008**, *97* (6), 2260−2276.

(5) Roggo, Y.; Chalus, P.; Maurer, L.; Lema-Martinez, C.; Edmond, A.; Jent, N. *J. Pharm. Biomed. Anal.* **2007**, *44* (3), 683−700.

(6) Vankeirsbilck, T.; Vercauteren, A.; Baeyens, W.; Van der Weken, G.; Verpoort, F.; Vergote, G.; Remon, J. P. *Trends Anal. Chem.* **2002**, *21* (12), 869−877.

(7) (a) Geppi, M.; Mollica, G.; Borsacchi, S.; Veracini, C. A. *Appl. Spectrosc. Rev.* **2008**, *43*, 202−302. (b) Vogt, F. G. *Future Med. Chem.* **2010**, *2* (6), 915−921.

(8) Chaires, J. B. *Annu. Rev. Biophys.* **2008**, *37* (1), 135−151.

(9) Istvan, E. S.; Deisenhofer, J. *Science* **2001**, *292* (5519), 1160−1164.

(10) Sonje, V. M.; Kumar, L.; Meena, C. L.; Kohli, G.; Puri, V.; Jain, R. *Atorvastatin Calcium. Profiles of Drug Substances, Excipients, and Related Methodology*; Elsevier Inc.: New York, 2010.

(11) Skorda, D.; Kontoyannis, C. G. *Talanta* **2008**, *74*, 1066−1070.

(12) Shete, G.; Puri, V.; Kumar, L.; Bansal, A. K. *AAPS PharmSciTech* **2010**, *11* (2), 598−609.

(13) Jin, Y. S.; Ulrich, J. *Chem. Eng. Technol.* **2010**, *33* (5), 839−844.
(14) (a) Zhang, H.; Ma, L. Patent C.CN101538237A, 2009. (b) Rafeeq, M.; Khan, A.; Mukarram, S. M. J. Patent I.IN2007MU01905A, 2010. (c) Rafeeq, M.; Khan, A.; Mukarram, S. M. J. Patent I.IN2007MU02159A, 2009. (d) Liu, Y.; Lin, X. Patent C.CN101684090A, 2010. (e) Kumar, Y.; Kumar, S. M. D.; Sathyanarayana, S. U.S. Patent 0,216,029 A1, 2009. (f) Jin, Y. S.; Joachim, U.; Choi, S. J.; Lee, B. G. Patent K.KR2011026831A, 2011. (g) Briggs, C. A. U.S. Patent 5,969,156, 1999.
(15) Brus, J.; Urbanova, M.; Sedenkova, I.; Brusova, H. *Int. J. Pharm.* **2011**, *409* (1−2), 62−74.
(16) (a) Harper, J. K.; Doebbler, J. A.; Jacques, E.; Grant, D. M.; Von Dreele, R. B. *J. Am. Chem. Soc.* **2010**, *132*, 2928−2937. (b) Harper, J. K.; Grant, D. M.; Zhang, Y.; Lee, P. L.; von Dreele, R. B. *J. Am. Chem. Soc.* **2006**, *128*, 1547−1552. (c) Harper, J. K.; Strohmeier, M.; Grant, D. M. *J. Magn. Reson.* **2007**, *189* (1), 20−31. (d) Heider, E. M.; Harper, J. K.; Grant, D. M. *Phys. Chem. Chem. Phys.* **2007**, *9* (46), 6083−6097. (e) Olejniczak, S.; Mikula-Pachoczyk, J.; Hughes, C. E.; Potrzebowski, M. J. *J. Phys. Chem.* **2008**, *122*, 1586−1593. (f) Olejniczak, S.; Potzebowski, M. J. *Org. Biomol. Chem.* **2004**, *2*, 2315−2322. (g) Smith, J.; MacMamara, E.; Raftery, D.; Borchardt, T.; Byrn, S. *J. Am. Chem. Soc.* **1998**, *120*, 11710−11713. (h) Smith, J.; Xu, W.; Raftery, D. *J. Phys. Chem. B* **2006**, *110*, 7766−7776. (i) Liu, W.; Wang, W. D.; Wang, W.; Bai, S.; Dybowski, C. *J. Phys. Chem. B* **2010**, *114* (49), 16641−16649.
(17) Rajeswaran, M.; Blanton, T. N.; Zumbulyadis, N.; Giesen, D. J.; Conesa-Moratilla, C.; Misture, S. T.; Stephens, P. W.; Huq, A. *J. Am. Chem. Soc.* **2002**, *124* (48), 14450−14459.
(18) Mafra, L.; Santos, S. M.; Siegel, R.; Alves, I.; Almeida Paz, F. A.; Dudenko, D.; Spiess, H. W. *J. Am. Chem. Soc.* **2012**, *134*, 71−74.
(19) Bennett, A. E.; Rienstra, C. M.; Auger, M.; Lakshmi, K. V.; Griffin, R. G. *J. Chem. Phys.* **1995**, *103*, 6951.
(20) Opella, S. J.; Frey, M. H. *J. Am. Chem. Soc.* **1979**, *101*, 5854−5856.
(21) van Rossum, B.-J.; Forster, H.; de Groot, H. J. M. *J. Magn. Reson.* **1997**, *124*, 516−519.
(22) Lee, M.; Goldburg, W. I. *Phys. Rev. A* **1965**, *140*, 1261.
(23) Liu, S.-F.; Mao, J.-D.; Schmidt-Rohr, K. *J. Magn. Reson.* **2002**, *155*, 15−28.
(24) (a) Dixon, W. T. *J. Magn. Reson.* **1981**, *44*, 220−223. (b) Dixon, W. T. *J. Chem. Phys.* **1982**, *77*, 1800−1809.
(25) Yates, J. R.; Dobbins, S. E.; Pickard, C. J.; Mauri, F.; Ghi, P. Y.; Harris, R. K. *Phys. Chem. Chem. Phys.* **2005**, *7*, 1402−1407.
(26) (a) Chen, Q.; Schmidt-Rohr, K. *Macromolecules* **2004**, *37* (16), 5995−6003. (b) Lee, Y. J.; Clark, C. G.; Graf, R.; Wagner, M.; Mullen, K.; Spiess, H. W. *J. Phys. Chem. B* **2009**, *113* (5), 1360−1366.
(27) Frisch, M. J.; Trucks, G. W.; Schlegel, H. B.; Scuseria, G. E.; Robb, M. A.; Cheeseman, J. R.; Scalmani, G.; Barone, V.; Mennucci, B.; Petersson, G. A.; Nakatsuji, H.; Caricato, M.; Li, X.; Hratchian, H. P.; Izmaylov, A. F.; Bloino, J.; Zheng, G.; Sonnenberg, J. L.; Hada, M.; Ehara, M.; Toyota, K.; Fukuda, R.; Hasegawa, J.; Ishida, M.; Nakajima, T.; Honda, Y.; Kitao, O.; Nakai, H.; Vreven, T.; Montgomery, J. A., Jr.; Peralta, J. E.; Ogliaro, F.; Bearpark, M.; Heyd, J. J.; Brothers, E.; Kudin, K. N.; Staroverov, V. N.; Kobayashi, R.; Normand, J.; Raghavachari, K.; Rendell, A.; Burant, J. C.; Iyengar, S. S.; Tomasi, J.; Cossi, M.; Rega, N.; Millam, J. M.; Klene, M.; Knox, J. E.; Cross, J. B.; Bakken, V.; Adamo, C.; Jaramillo, J.; Gomperts, R.; Stratmann, R. E.; Yazyev, O.; Austin, A. J.; Cammi, R.; Pomelli, C.; Ochterski, J. W.; Martin, R. L.; Morokuma, K.; Zakrzewski, V. G.; Voth, G. A.; Salvador, P.; Dannenberg, J. J.; Dapprich, S.; Daniels, A. D.; Farkas, O.; Foresman, J. B.; Ortiz, J. V.; Cioslowski, J.; Fox, D. J. *Gaussian 09*, revision C.01; Gaussian, Inc.: Wallingford, CT, 2009.
(28) Kim, M. S.; Jin, S. J.; Kim, J. S.; Park, H. J.; Song, H. S.; Neubert, R. H. H.; Hwang, S. J. *Eur. J. Pharm. Biopharm.* **2008**, *69* (2), 454−465.
(29) Herzfeld, J.; Berger, A. E. *J. Chem. Phys.* **1980**, *73*, 6021−6031.
(30) Senkovska, I.; Thewalt, U. *Acta Crystallogr., Sect. C: Cryst. Struct. Commun.* **2005**, *61*, M448−M449.
(31) Klop, E. A.; Schouten, A.; Van Der Sluis, P.; Spek, A. L. *Acta Crystallogr., Sect. C: Cryst. Struct. Commun.* **1984**, *C40*, 51−53.
(32) (a) Alderman, D. W.; McGeorge, G.; Hu, J. Z.; Pugmire, R. J.; Grant, D. M. *Mol. Phys.* **1998**, *95*, 1113−1126. (b) Antzutkin, O. N.; Shekar, S. C.; Levitt, M. H. *J. Magn. Reson., Ser. A* **1995**, *115*, 7−19. (c) Antzutkin, O. N.; Shekar, S. C.; Levitt, M. H. *J. Magn. Reson.* **1998**, *135*, 144−155. (d) Chan, J. C. C.; Tycko, R. *J. Chem. Phys.* **2003**, *118*, 8378.
(33) (a) Gu, Z.; McDermott, A. E. *J. Am. Chem. Soc.* **1993**, *115*, 4282−4285. (b) Gu, Z.; Zambrano, R.; McDermott, A. E. *J. Am. Chem. Soc.* **1994**, *111*, 6368−6372. (c) Wei, Y. F.; Lee, D. K.; Rammamoorthy, A. *J. Am. Chem. Soc.* **2001**, *123*, 6118−6126.
(34) Laurencin, D.; Gervais, C.; Wong, A.; Coelho, C.; Mauri, F.; Massiot, D.; Smith, M. E.; Bonhomme, C. *J. Am. Chem. Soc.* **2009**, *131* (37), 13430−13440.